Atmos. Chem. Phys., 25, 1105–1119, 2025
https://doi.org/10.5194/acp-25-1105-2025

Atmospheric Chemistry and Physics
Open Access
EGU

Research article

Preindustrial-to-present-day changes in atmospheric carbon monoxide: agreement and gaps between ice archives and global model reconstructions

Xavier Faïn[1], Sophie Szopa[2], Vaishali Naïk[3], Patricia Martinerie[1], David M. Etheridge[4,5], Rachael H. Rhodes[6], Cathy M. Trudinger[4,5], Vasilii V. Petrenko[7], Kévin Fourteau[8], and Philip Place[7,a]

[1]Univ. Grenoble Alpes, CNRS, INRAE, IRD, Grenoble INP, IGE, 38000 Grenoble, France
[2]Laboratoire des Sciences du Climat et de l'Environnement, CEA, CNRS, UVSQ, Université Paris-Saclay, Gif-sur-Yvette, France
[3]NOAA Geophysical Fluid Dynamics Laboratory, Princeton, NJ, USA
[4]CSIRO Environment, Aspendale, Victoria, Australia
[5]Australian Antarctic Program Partnership, Institute for Marine and Antarctic Studies, University of Tasmania, Hobart, Tasmania, Australia
[6]Department of Earth Sciences, University of Cambridge, Cambridge, CB2 3EQ, UK
[7]Department of Earth and Environmental Sciences, University of Rochester, Rochester, NY 14627, USA
[8]Univ. Grenoble Alpes, Université de Toulouse, Météo-France, CNRS, CNRM, Centre d'Études de la Neige, Grenoble, France
[a]present address: University Instrumentation Center, University of New Hampshire, Durham, NH 03824, USA

Correspondence: Xavier Faïn (xavier.fain@univ-grenoble-alpes.fr)

Received: 4 March 2024 – Discussion started: 17 April 2024
Revised: 25 October 2024 – Accepted: 22 November 2024 – Published: 28 January 2025

Abstract. Global chemistry–climate models (CCMs) play an important role in assessing the climate and air pollution implications of aerosols and chemically reactive gases. Evaluating these models under past conditions and constraining historical sources and sinks necessitate reliable records of atmospheric mixing ratios spanning preindustrial times. Such precious records were recently obtained for carbon monoxide (CO), documenting for the first time the evolution of this reactive compound over the industrial era. In this study, we compare the simulated atmospheric surface CO mixing ratios ([CO]) from two different sets of chemistry–climate models and emissions within the frameworks of CMIP5 and of CMIP6 (Coupled Model Intercomparison Project Phases 5 and 6) to recent bipolar ice archive reconstructions for the period spanning 1850 to the present. We analyse how historical (1850–2014) [CO] outputs from 16 ACCMIP (Atmospheric Chemistry and Climate Model Intercomparison Project) models and 7 AerChemMIP (Aerosol Chemistry Model Intercomparison Project) models over Greenland and Antarctica are able to capture both absolute values and trends recorded in multi-site ice archives. While most models underestimate [CO] at northern high latitudes, a reduction in this bias is observed between the ACCMIP and the AerChemMIP exercise. Over the 1980–2010 CE period (common era; all subsequent years in the paper are reported in CE), trends in ice archive and firn air observations and AerChemMIP outputs align remarkably well at northern and southern high latitudes, indicating improved quantification of anthropogenic CO emissions and the main CO sink (OH oxidation) compared to ACCMIP. From 1850 to 1980, AerChemMIP models and observations consistently show increasing [CO] in both the Northern Hemisphere (NH) and Southern Hemisphere (SH), suggesting a robust understanding of the CO budget evolution. However, a divergence in the [CO] growth rate emerges in the NH between models and observations over the 1920–1980 period, attributed to uncertainties in CO emission factors (EFs), particularly EFs for the RCO (residential, commercial, and other) and transportation sectors, although we cannot totally rule out the possibility that the CO record based on the Greenland ice archives may be biased high by CO chemical production processes occurring in the ice prior

to the measurements (i.e. in situ CO production). In the Southern Hemisphere, AerChemMIP models simulate an increase in atmospheric [CO] from 1850 to 1980 that closely reproduces the observations (22 ± 10 ppb and 13 ± 7 ppb, respectively). Such agreement supports CMIP6 biomass burning CO emission inventories, which do not reveal a peak in CO emissions in the late 19th century. Furthermore, both SH models and observations reveal an accelerated growth rate in [CO] during 1945–1980 relative to 1850–1945, likely linked to increased anthropogenic transportation emissions.

1 Introduction

Carbon monoxide (CO) is an air pollutant that affects the oxidizing capacity of the troposphere and contributes to ozone formation (Crutzen, 1973). Its primary loss is through reaction with OH, with a small contribution from dry deposition, which leads to an atmospheric lifetime of about 2 months (Khalil et al., 1999). Thus, CO is an excellent tracer of long-range transport and an integrator of atmospheric chemical processes. In the modern atmosphere, the main sources of CO are combustion (fossil fuel and biomass burning) and secondary production in the atmosphere (atmospheric oxidation of methane (CH_4) and non-methane volatile organic compounds (VOCs)). Methane oxidation currently amounts to 70 %–80 % of the secondary atmospheric CO production (Duncan et al., 2007; Fortems-Cheiney et al., 2012). CO surface emissions include biomass burning (van der Werf et al., 2017), incomplete combustion of anthropogenic fossil fuels and biofuels (Hoesly et al., 2018), and minor contributions from the ocean (Conte et al., 2019) and plant leaves (Bruhn et al., 2013). Incomplete fossil fuel combustion represents ∼ 70 % of primary CO emissions (Szopa et al., 2021, and references therein). A schematic overview of the modern global CO budget is given in Fig. 1.

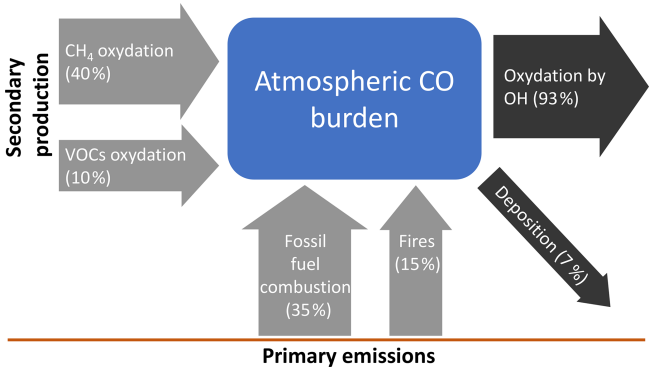

Figure 1. The modern budget of atmospheric CO. Primary emissions and secondary production each amount to ∼ 50 % of CO sources (Szopa et al., 2021). Primary emissions for plant leaves and oceans are small and are not shown here; the proportions of emissions from fossil fuel combustion and fires are 35 % and 15 %, respectively (Szopa et al., 2021). Secondary CO production is dominated by CH_4 oxidation, which amounts to ∼ 35 %–40 % of the global CO source, with VOC oxidation accounting for ∼ 10 %–15 % (Duncan et al., 2007; Fortems-Cheiney et al., 2012). The main CO sink is through OH oxidation, which accounts for more than 90 % of CO removal (Khalil et al., 1999; Stein et al., 2014).

Recent advances in satellite retrievals, ground-based column observations, airborne platforms, surface measurement networks, and assimilation products have improved the characterization of the present-day atmospheric CO distribution (Szopa et al., 2021, and references therein). Typical annual mean surface CO concentrations range from ∼ 120 ppb in the Northern Hemisphere (NH) to ∼ 40 ppb in the Southern Hemisphere (SH) (Petron et al., 2023). A study using data assimilation techniques estimates a global mean CO burden of 356 ± 27 Tg over the 2002–2013 CE (common era; all subsequent years in the paper are reported in CE) period (Gaubert et al., 2017). There is high confidence that the global CO burden has been declining since 2000 (Szopa et al., 2021, and references therein), although this decreasing global trend in CO has slowed down over the last 5 years (Buchholz et al., 2021; Petron et al., 2023).

Recent analytical and modelling advances applied to ice archives (firn air and bubbles trapped in deep ice) from both Greenland (Petrenko et al., 2013; Faïn et al., 2022a) and Antarctica (Faïn et al., 2023a; Strawson et al., 2024) have allowed the production of a new bipolar reconstruction of atmospheric carbon monoxide, including preindustrial (PI) times, and spanning 1700–1992 (1700–2016) in the SH (in the NH). These reconstructions can be extended to the present day using direct measurements of atmospheric [CO] at high latitudes, e.g. at the Mawson or South Pole stations (Antarctica) and at the Kennaook / Cape Grim station (Australia) in the SH (Faïn et al., 2023a; Loh et al., 2021).

Estimates of global anthropogenic emissions of both CO and its precursors have been revised recently for use in the Coupled Model Intercomparison Project Phase 6 (CMIP6; Collins et al., 2017). Hoesly et al. (2018) have extended these estimates of anthropogenic emissions back to 1750 and developed differentiation (by source sector) and gridding of emissions (Feng et al., 2020). Similarly, biomass burning CO emissions, which represent about 30 % of present-day global CO emissions (i.e. about 15 % of global CO sources, Fig. 1), have been revised in the framework of CMIP6 (van Marle et al., 2017). CMIP6 biomass burning CO emissions, which assume that fires scale up with population density, increase only slightly from 1750 to 2015 and peak during the 1990s, after which they decrease gradually and consistently.

However, fire emissions that reach higher levels in PI times compared to the present day have been recently suggested (Hamilton et al., 2018; Liu et al., 2021; Rowlinson et al., 2020) as a result of a possible decline in burned areas with increasing population density due to land use changes (Andela et al., 2017; Knorr et al., 2014).

CMIP6-updated anthropogenic and biomass burning CO emissions inventories have been used by a set of state-of-the-art global chemistry–climate models (CCMs) to investigate the trends in global tropospheric hydroxyl radical and methane's lifetime (Stevenson et al., 2020) and the evolution of the tropospheric ozone burden and budget terms (Griffiths et al., 2021) since 1850. Chemistry–climate models suggest that the global tropospheric CO burden has increased by ~ 120 Tg since 1850 (Fig. 1 in Griffiths et al., 2021), with (i) a moderately increasing rate from 1850 to 1950, (ii) a quickly increasing rate from 1950 to 1990, and (iii) a decreasing trend from 1990 to 2015 that reproduces the observed decline in tropospheric [CO] (Szopa et al., 2021, and references therein).

In this paper, we compare trends in atmospheric surface [CO] simulated by two different sets of CCMs and emissions within the framework of CMIP5 (Lamarque et al., 2013) and CMIP6 to recent reconstructions from polar ice archives for the period spanning 1850 to the present. The aim of this work is to establish the periods of robust agreement between models and data, indicating a robust knowledge of trends in emissions and adequate fitness of the models over such periods, and to discuss the possible reasons for disagreement over specific periods.

2 Bipolar [CO] reconstructions from polar ice archives

Ground-based and satellite-derived CO data are only available for the last 3 decades. Ancient air preserved in glacial ice and firn is thus a unique archive for reconstructing the past atmospheric [CO] record prior to the 1990s. A large amount of air can be sampled from the interconnected open pores of the firn, which is the upper layer of an ice sheet where snow is slowly transformed into ice. Mean ages of atmospheric gases increase to about a century ago with firn depth. Analysis of air trapped in bubbles in solid ice below the firn layer is required to extend reconstructions further back in time and can now be conducted by continuous flow analysis (CFA), which produces continuous, high-resolution datasets (Faïn et al., 2023a, 2022a, 2014).

By analysing [CO] depth profiles collected from firn air at three different Greenland sites (NGRIP, Summit, and NEEM), Petrenko et al. (2013) obtained a reconstruction of atmospheric [CO] spanning 1950–2010. Over the same period, stable isotopes of CO (i.e. δ^{13}CO and δC^{18}O) were analysed in firn air samples collected at the NEEM site to provide additional powerful clues to the interpretation of the changes in the CO budget (Wang et al., 2012). The reconstruction from Petrenko et al. (2013) has recently been extended back to 1700, with the CFAs of four different Greenland ice cores (Fig. 2, upper panel: NGRIP, PLACE, NEEM, and D4) (Faïn et al., 2022a). Faïn et al. (2022a) could not fully exclude the possibility that the Greenland ice archive CO reconstruction could be slightly positively biased by chemical processes (in situ production) occurring within the Greenland ice. Therefore, the atmospheric [CO] history extracted from Greenland should be considered an upper bound of the past [CO] in the Arctic (Faïn et al., 2022a). The temporal changes depicted by this historical Greenland [CO] record probably have a larger spatial significance than the Arctic context alone, as suggested by the GAW (Global Atmospheric Watch) reactive gas measurement network (Petron et al., 2023; Schultz et al., 2015).

Ice archives from Antarctica were also investigated: CO was collected from firn air at seven sites (Lock In, DE08-2, DSSW19K, DSSW20K, the South Pole, ABN, and Berkner Island) to reconstruct [CO] in the Antarctic atmosphere from 1898 to the present (Fig. 2, lower panel; Faïn et al., 2023a). CFAs conducted on three ice cores (DC12, ABN, and TaldIce) extended this reconstruction backward for 3 millennia, starting in 1897 (Faïn et al., 2023a). Ice core and firn air measurements, as well as firn air and direct atmospheric measurements, show excellent agreement during intervals of overlap. These Antarctic CO records appear to be unaffected by in situ CO production or sampling artifacts and are in excellent agreement with a recent ice core CO record from the Antarctic Peninsula spanning 1821–1995 (Fig. 2; Strawson et al., 2024), although the peninsular CO record reveals multidecadal variability due to higher accumulation of ice archives. These new Antarctic CO reconstructions suggest that the previously published Antarctic [CO] datasets (Haan et al., 1996; Haan and Raynaud, 1998; Wang et al., 2010) were likely biased high. The [CO] reconstruction based on Antarctic ice archives reported in Fig. 2 is representative of the 45–90° S atmosphere, with temporal changes probably having a larger spatial significance, including at least the 30–90° S latitudinal band (Faïn et al., 2023a).

3 The ACCMIP exercise

The Atmospheric Chemistry and Climate Model Intercomparison Project (ACCMIP), which was part of CMIP5, consisted of a series of time slice experiments to investigate long-term changes in atmospheric composition between 1850 and 2100 and how composition changes impact radiative forcing (Lamarque et al., 2013).

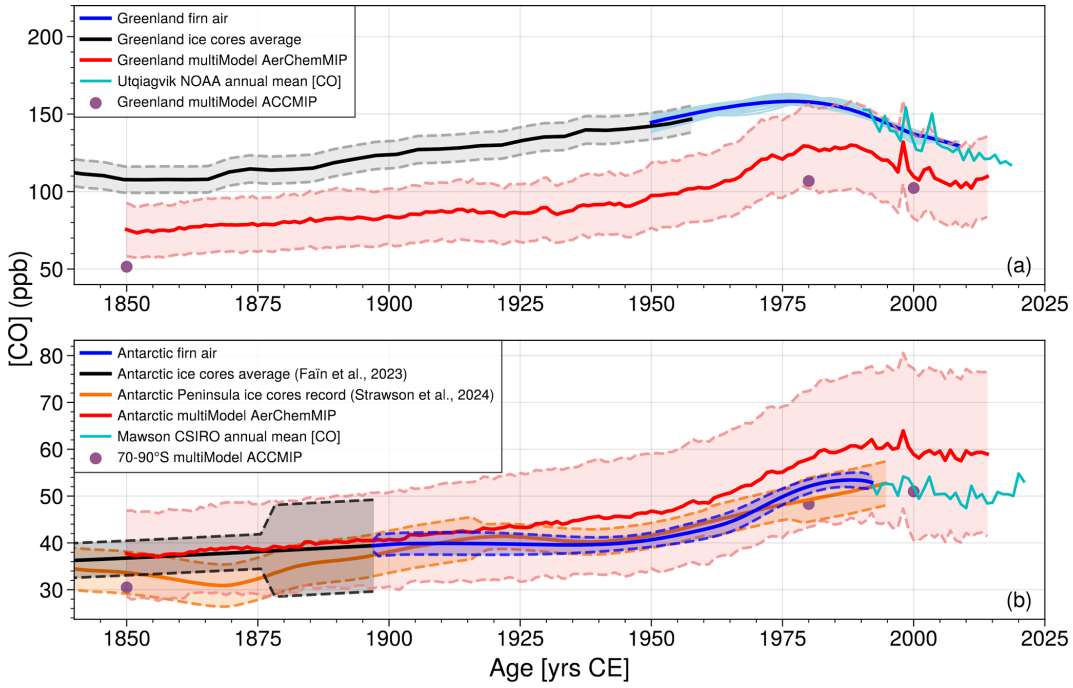

Figure 2. Greenland **(a)** and Antarctic **(b)** atmospheric [CO] from ice cores and firn air reconstructions (Faïn et al., 2023a, 2022a; Petrenko et al., 2013), from NOAA and CSIRO atmospheric monitoring, and from multimodel AerChemMIP historical [CO] simulations (red line). The grey envelope on the Greenland (Antarctic) ice core [CO] record reports the 1σ (2σ) uncertainty (Faïn et al., 2023a, 2022a). In the upper panel, **(a)**, light blue denotes the firn air records obtained by combining samples from three Greenland sites and is a metric of the uncertainty, and blue represents the average firn air record (Petrenko et al., 2013). In the lower panel, **(b)**, the blue envelope on the Antarctic firn air [CO] reconstruction reports 2σ uncertainty. The recent CO record from the Antarctic Peninsula (Strawson et al., 2024) is shown in orange, with a combined 2σ uncertainty envelope. The red envelopes on the AerChemMIP simulations show 1σ uncertainties. The multimodel ACCMIP [CO] is also reported for 1850, 1980, and 2000.

3.1 ACCMIP CO budget

3.1.1 CO sources

Anthropogenic and biomass burning CO emissions used within the framework of ACCMIP are taken from the RETRO and EDGAR-HYDE inventories (Lamarque et al., 2010). Natural emissions for CO were specified from different sources depending on the models.

3.1.2 CO sinks

Sinks for atmospheric CO include oxidation with OH radicals and CO uptake via oxidation by soil microbes. Reaction with OH radicals acts as the major CO sink, while deposition in the soil contributes about 10 % to the global atmospheric CO losses (Duncan et al., 2007; Khalil et al., 1999; Stein et al., 2014). ACCMIP models exhibit a large diversity in the magnitude and sign of PI times compared to present-day OH changes (ranging from a decrease of 12.7 % to an increase of 14.6 %). Despite large regional changes, the multimodel global mean (mass-weighted) OH concentration changes little over the past 150 years (Naik et al., 2013). For the 1980 to 2000 period, ACCMIP models find a slight increase in mean OH (3.5 % ± 2.2 %) (Naik et al., 2013).

3.2 Model outputs

In this study, we extract historical CO mixing ratio outputs from the 16 ACCMIP models (Naik et al., 2013) available at the Comprehensive Environmental Data Archive (CEDA) dataset repository (https://catalogue.ceda.ac.uk/, last access: August 2021) for three time slices (1850, 1980, and 2000) over two areas: (i) Greenland (60–20° W, 84–60° N) and (ii) Antarctica (90–70° S). For each time slice, a single multimodel mean [CO] is obtained by averaging CO outputs of the 16 models. Figure 2 (Fig. 3) reports the ACCMIP multimodel absolute CO levels (the [CO] anomaly relative to 2000) for both Arctic and Antarctic atmospheres (in ppb).

4 The AerChemMIP exercise

The Aerosol Chemistry Model Intercomparison Project (AerChemMIP) is part of CMIP6 and aims to quantify the climate and air quality impacts of aerosols and chemically reactive gases, including CO (Collins et al., 2017). In this

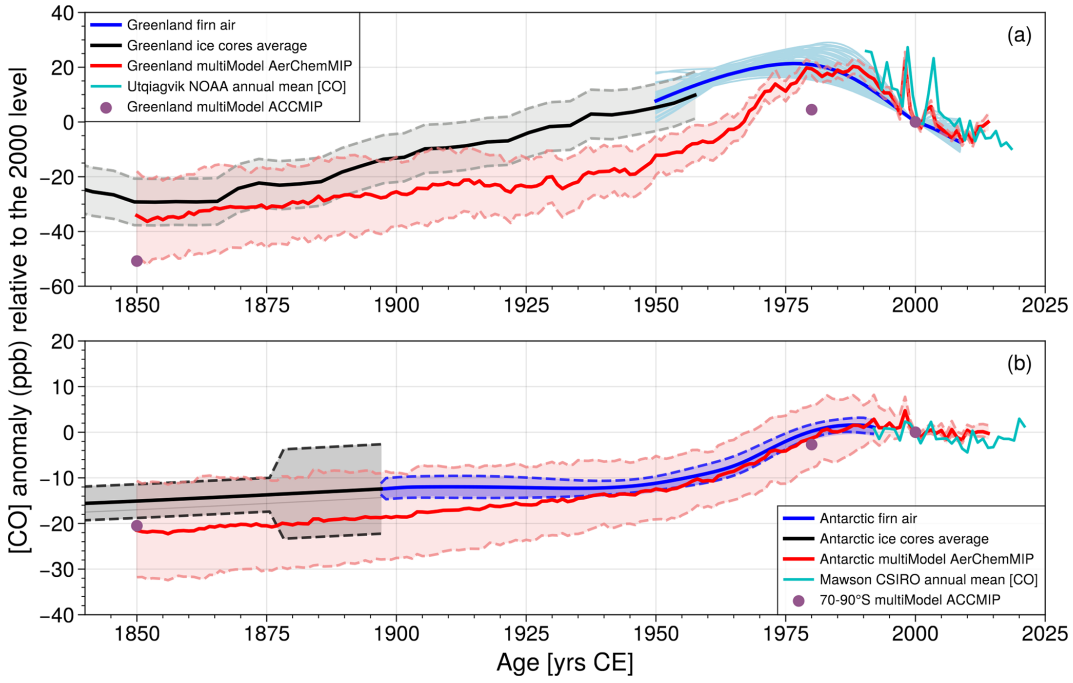

Figure 3. Anomaly of Greenland **(a)** and Antarctic **(b)** atmospheric [CO] from ice cores and firn air reconstructions (Faïn et al., 2023a, 2022a; Petrenko et al., 2013), from NOAA and CSIRO atmospheric monitoring, and from multimodel AerChemMIP historical simulations (red line). The grey envelope on the Greenland (Antarctic) ice core [CO] record reports 1σ (2σ) uncertainty (Faïn et al., 2023a, 2022a). In the upper panel, **(a)**, light blue denotes the firn air records obtained by combining samples from three Greenland sites and is a metric of the uncertainty, and blue represents the average firn air record (Petrenko et al., 2013). In the lower panel, **(b)**, the blue envelope on the Antarctic firn air [CO] reconstruction reports 2σ uncertainty. The red envelopes on the multimodel AerChemMIP simulations show 1σ uncertainties. The multimodel ACCMIP [CO] anomaly is also reported for 1850, 1980, and 2000. All data are reported as anomalies relative to annually averaged levels from the year 2000.

study, we use the historical (1850–2014) CO mixing ratio outputs from seven models involved in the AerChemMIP exercise: UKESM1-0-LL (Archibald et al., 2020), GFDL-ESM4 (Dunne et al., 2020; Horowitz et al., 2020), CESM2-WACCM (Emmons et al., 2020), BCC-ESM1 (Zhang et al., 2021; Wu et al., 2020), GISS-E2 (Bauer et al., 2020), MRI-ESM2 (Yukimoto et al., 2019), and EC-Earth3 (van Noije et al., 2021). No criteria were applied to select specific models, and we included in this study all CO modelling results available on the Earth System Grid Federation (ESGF) dataset repository at the end of July 2024.

4.1 AerChemMIP CO budget

4.1.1 CO sources

Anthropogenic and biomass burning CO emissions used in the framework of AerChemMIP have recently been produced specifically for CMIP6 for the 1750–2014 period and are common to all models. Anthropogenic CO emissions are reported by Hoesly et al. (2018) and include emissions from aircraft; energy production; industry; residential, commercial, and other (RCO); shipping; transportation on land; and waste (including waste burning). Biomass burning CO emissions are based on merging satellite observations with proxies and fire models (van Marle et al., 2017).

Biogenic sources are not constrained by the AerChemMIP protocol. Biogenic VOC (BVOC) emissions are often interactive: CESM2, GFDL, and BCC models use the same emission model (MEGAN; Guenther et al., 2006), while UKESM1 or GISS-E2 apply different models (Pacifico et al., 2011, and Shindell et al., 2006, respectively). MRI-ESM2 and EC-Earth3 models prescribe constant BVOC emissions (Oshima et al., 2020; van Noije et al., 2021). A comparison of BVOC emissions for five of the models involved in this study is provided by Griffiths et al. (2021, Fig. 1). The direct CO emission from biogenic sources (e.g. plant leaves) is low, but the emissions of biogenic VOCs (BVOCs), later oxidized into CO, are a large source of atmospheric CO (Fig. 1).

For all models, CH_4 mixing ratios are prescribed at ground levels using ice core reconstructions (Meinshausen et al., 2017). The CH_4 oxidation CO source is thus well constrained in terms of the trend but can vary accordingly to the absolute OH values, which differ from one model to another.

4.1.2 CO sinks

AerChemMIP models simulate stable global OH from 1850 to 1980 and a 10 % increase in global OH since 1980, indicating that no changes in the major CO sink are modelled prior to 1980 (Stevenson et al., 2020). However, spatial distribution of the OH radical, which differs among models (Stevenson et al., 2020), can have a large impact on the main CO sink (Strode et al., 2015).

Although much smaller, the CO sink driven by dry deposition into soil is included in the AerChemMIP models (e.g. Archibald et al., 2020; Emmons et al., 2020; Horowitz et al., 2020). However, this CO sink remains poorly constrained, as little focus has been placed so far on the role of CO dry deposition in global modelling (Stein et al., 2014).

4.2 Model outputs

In this study, we extract historical (1850–2014) CO mixing ratio outputs from the seven AerChemMIP models mentioned earlier over the same two areas already defined for the ACCMIP simulation (Sect. 3.2): (i) Greenland (60–20° W, 84–60° N) and (ii) Antarctica (90–70° S). For each model, we first obtain a single time series by averaging all members available on the ESGF dataset repository (https://aims2.llnl.gov/search, last access: July 2024) at the end of July 2024. For each area (Greenland and Antarctica), model outputs are thus combined to produce (i) a multimodel history of absolute [CO] (Fig. 2, red line) and (ii) a multimodel [CO] trend defined as the [CO] anomaly relative to the 2000 [CO] level (Fig. 3, red line). The envelopes reported in Figs. 2 and 3 (1σ) represent the variability in simulated [CO] among the seven models and can be interpreted as the uncertainty in how state-of-the-art CCMs can simulate historical [CO]. Individual model outputs are reported in Figs. S1 (Greenland) and S2 (Antarctica) in the Supplement. Interestingly, while differences in transport dynamics and chemical schemes (e.g. Shindell et al., 2006) drive a wide range of CO burdens among models, they do not drive a large diversity in modelled trends (Figs. S1 and S2). One of the seven models, the BCC-ESM1 model, exhibits a larger CO burden, but excluding this outlier model has little effect on the multimodel mean results.

5 New insights into the past CO budget

In this section, we compare observations (i.e. historical reconstructions retrieved from ice archives, Sect. 2) to ACCMIP and AerChemMIP multimodel outputs (Sects. 3 and 4) at both northern and southern high latitudes to infer new constraints on past CO sources and sinks.

5.1 Model bias of [CO] at high latitudes

We observe discrepancies in absolute [CO] values between model output and ice archive datasets (Fig. 2). The AerChemMIP model mean is about 20 % lower than ice archive datasets at northern high latitudes during the entire 1850–2014 period. At southern high latitudes, the AerChemMIP model mean is in good agreement with the ice archive dataset during the period spanning 1850–1900, with a positive bias slowly increasing from 1900 to 1970 to reach modelled [CO] about 20 % higher than that in ice core archives during the last 3 decades. Such discrepancies also exist for the most recent 2 decades in surface ground observations (e.g. at Utqiaġvik (formerly Barrow), Alaska, USA, and Mawson Station, Antarctica; Fig. 2). However, the AerChemMIP model mean agrees with the ice core record from Antarctica within its 1σ variability envelope, and we thus focus here on the NH [CO] model bias.

The negative bias in the AerChemMIP model mean [CO] at northern middle-to-high latitudes (Fig. 2) is consistent with the systematic underestimation of observed [CO] at these latitudes, but the hypotheses to explain such a bias vary between studies. Missing anthropogenic emissions from the inventories are commonly given as a hypothesis to explain the negative CO bias (e.g. Emmons et al., 2020; Heimann et al., 2020; Miyazaki et al., 2020; Shindell et al., 2006; Stein et al., 2014). However, underestimation of the secondary CO production from the chemical oxidation of methane or VOCs could also be involved (e.g. Archibald et al., 2020; Gaubert et al., 2017; Heimann et al., 2020), as well as CO losses via OH oxidation (Archibald et al., 2020; Strode et al., 2015) or soil deposition (Stein et al., 2014). Recent studies have suggested mitigating the negative CO bias in the NH by assimilating multiple datasets of chemical observations (e.g. Gaubert et al., 2020; Miyazaki et al., 2020; Zheng et al., 2019). The causes of negative CO biases at northern middle-to-high latitudes in CCMs remain highly debated, but targeted sensitivity experiments for bias attribution are outside the scope of this study. However, how models represent absolute [CO] at northern latitudes has improved over the last decade, as shown by the reduction in the negative bias in model mean [CO] between the ACCMIP and the AerChemMIP exercises (Fig. 2). Furthermore, not all models exhibit a negative bias at northern high latitudes; for example, the UKESM1 model accurately simulates the absolute [CO] observed at Utqiaġvik (formerly Barrow, AK) over the last 3 decades, and the BCC-ESM1 model shows a positive bias (Fig. S1).

5.2 Global decline in atmospheric [CO] since 1990

Over the period spanning 1990–2010, trends in observations and AerChemMIP multimodel outputs are in excellent agreement at both northern and southern high latitudes (Fig. 3). Trends in atmospheric [CO] are defined here as variations in [CO] relative to the year 2000. In the SH, the [CO] trend ob-

served at Mawson Station (-0.15 ± 0.04 ppb yr^{-1}, 1σ, $p < 0.01$) agrees within its uncertainty range with the AerChemMIP multimodel [CO] trend (-0.20 ± 0.07 ppb yr^{-1}, 1σ, $p < 0.01$). In the NH, [CO] trends are almost identical between atmospheric monitoring (Utqiaġvik (formerly Barrow), -1.27 ± 0.16 ppb yr^{-1}, 1σ, $p < 0.01$), Greenland firn air reconstruction (-1.14 ± 0.01 ppb yr^{-1}, 1σ, $p < 0.01$), and models (-1.22 ± 0.16 ppb yr^{-1}, 1σ, $p < 0.01$) during the 1990–2010 period. Isotopic CO analysis conducted on Greenland firn air suggests that the decline in Arctic [CO] between the peak in the 1970s and 2000 is due almost entirely to reduced fossil fuel emissions, specifically reductions from road transportation (Wang et al., 2012). Over the recent decades, AerChemMIP models also successfully capture the amplitude and phase of the [CO] seasonal cycle at different latitudes, as well as the magnitude of interannual variability in atmospheric [CO] revealed by direct atmospheric monitoring (Archibald et al., 2020; Emmons et al., 2020; Horowitz et al., 2020). Figure 3 reveals how AerChemMIP models reproduce interannual variability in Arctic [CO] driven by biomass burning (e.g. during summer 1998). Such variability is not captured by ice archives due to the temporal smoothing introduced by gas diffusion in polar firn.

Recent decades are when surface emissions of CO are the best constrained (Hoesly et al., 2018). Non-methane VOC (NMVOC) emissions are also precisely quantified (Hoesly et al., 2018), and atmospheric [CH_4] is prescribed using ice core records (Meinshausen et al., 2017); thus, secondary CO production is also well known. The good agreement in the trends between model outputs and observations suggests that the main CO sink (OH oxidation) is also accurately represented within models. AerChemMIP models report stable global levels of tropospheric OH from 1850 to 1980 and a $\sim 10\,\%$ increase in OH from 1980 to 2014 (Fig. 2a from Stevenson et al., 2020). The good agreement in the trends between models and observations reported here lends credibility to the OH trend simulated by AerChemMIP models. It also suggests that the recent increase in anthropogenic NO_x emission is well understood.

Figure 3 also includes a comparison between AerChemMIP and ACCMIP modelling outputs, with ACCMIP temporal resolution being much more limited. The ACCMIP multimodel simulation of the Arctic [CO] is only 4 ppb lower in 2000 compared to 1980 (Naik et al., 2013). ACCMIP models were not able to fully reproduce the decline in Arctic [CO] reconstructed for the last decade. Petrenko et al. (2013) already reported poor agreement between the trends from a firn air [CO] record and a CAM-Chem historical run, which was part of the ACCMIP exercise. One possible reason for such improvement in the framework of AerChemMIP is the anthropogenic emissions dominant over the last decades, which are better constrained now (Hoesly et al., 2018). Also, modelled trends in secondary CO sources (notably oxidation of VOCs) are difficult to compare across the different generations of models because of the lack of required outputs. Since models vary in their representation of the chemical mechanisms (and therefore VOC chemistry), we expect this to be a driving factor in the diversity of CO trends, similar to that for O_3 (Young et al., 2013; Griffiths et al., 2021). Additionally, trends in OH, which is the primary sink for CO, also vary across the models (Naik et al., 2013; Stevenson et al., 2020). Analysing the inter-exercise (ACCMIP vs. AerChemMIP) and inter-model (see Sect. 5.1) differences in atmospheric [CO] levels would require more outputs from the models that have not been archived and sometimes would require extra simulations, which are beyond the scope of this study.

5.3 Increase in Northern Hemisphere atmospheric [CO] from 1850 to 1980

During the time period spanning 1850–1980, both AerChemMIP models and observations exhibit increasing [CO] (Figs. 2 and 3). At northern latitudes, the increase in [CO] simulated from 1850 to 1980 is ~ 55 ppb, in excellent agreement with observations that reveal a ~ 50 ppb increase for this period. NH simulated and observed trends in [CO] agree within their 1σ uncertainties prior to 1920 but diverge during the 1920–1980 period. While the ice core and firn-based records exhibit an increase in [CO] at a steady rate of ~ 0.5 ppb yr^{-1}, the AerChemMIP multimodel average reveals slow growth from 1920 to 1945, at a rate of ~ 0.2 ppb yr^{-1}, which quickens from 1945 to 1980, at a rate of ~ 1.1 ppb yr^{-1}. At southern latitudes, AerChemMIP models simulate a larger increase in atmospheric [CO] from 1850 to 1980 than observations (22 ± 10 ppb and 13 ± 7 ppb, respectively), although model outputs and ice archive datasets always agree within their 1σ uncertainties. Both models and observations also reveal an increase in [CO] growth rate in the SH, which is twice as large between 1945 and 1980 as it was between 1850 and 1945. Finally, over the time period spanning 1850–1980, the [CO] trends simulated by the ACCMIP datasets are similar to those produced within the framework of AerChemMIP (Fig. 3). For this period, a key improvement of AerChemMIP compared to ACCMIP is the annual resolution of the model runs.

The general agreement between simulated and observed [CO] trends in both the NH and SH for the period spanning 1850–1980 indicates a good overall understanding of the evolution of the CO budget over this period. However, a mismatch in [CO] trends remains between the AerChemMIP multimodel mean and the ice archive dataset in the NH for the period spanning 1920 to 1980, with the multimodel mean showing a lower trend before 1945 and a higher trend after 1945 (Fig. 3). The CO record based on the Greenland ice archives should be considered an upper bound of the past CO abundance, and we cannot fully rule out the possibility that in situ production artifacts (Faïn et al., 2022a) impacting ice and firn air samples explain such a mismatch (Sect. 2). However, the Greenland ice archive record is a combination of five ice core and three firn air records, which all support

an increase in [CO] at a steady rate during the 1920–1980 period (Faïn et al., 2022a). We thus investigate whether uncertainties in descriptions of the CO sources and sinks used by AerChemMIP models can explain the differences in the [CO] growth rate between models and observations for the period spanning 1920–1980.

5.3.1 OH oxidation CO sink

A first hypothesis to explain the differences in trends between ice archive and model [CO] in the NH for the period spanning 1920–1980 could be an inaccurate estimation of the OH oxidation CO sink by models. AerChemMIP simulations suggest that the global tropospheric hydroxyl radical changes little from 1850 to 1980 (Stevenson et al., 2020). Global OH reconstructions are not easily comparable with Greenland [CO] reconstructions because OH is more abundant in the tropics, whereas the latitudinal band that is of most importance for polar CO is considerably narrower, likely $\sim$ 30–90° because of the relatively short atmospheric lifetime of CO. Ozone precursor (NO_x, CO, and VOC) emissions have strongly influenced OH trends; in particular, the relative roles of changing emissions of CO and NO_x have important competing consequences. Higher concentrations of NO_x increase OH through ozone photochemical production and the subsequent reaction with H_2O to produce OH, as well as the recycling of HO_2 to OH. On the other hand, higher concentrations of CO and VOCs (and CH_4) will reduce OH. Stevenson et al. (2020) report a dominant role of NO_x emission increases, whose impact overwhelms the impacts of increasing CO (up to the 1990s) and VOC emissions, which have tended to reduce OH. Finally, the OH oxidation CO sink modelled in the framework of AerChemMIP is closely related to NO_x emission inventories. To reconcile modelled and ice-core-based NH CO trends, a decrease in the OH oxidation CO sink would be required during the period spanning 1870–1945, which would mean lower NO_x emissions. The CMIP6 NO_x emissions remain low before 1945 (Fig. 1 in Stevenson et al., 2020). Considering the period spanning 1945–1980, an increase in the OH oxidation CO sink would be required to reconcile modelled and observed [CO] growth rates. Overall, if an inaccurate estimation of the OH oxidation CO sink by models was the cause of the mismatch between the observed and modelled NH [CO] trends, it would imply centennial variation in global OH, with improbably low OH levels in the early 20th century. A diversity of models is involved here (i.e. diversity of chemical schemes), and the drivers of variability in global OH can be very different between models (Wild et al., 2020). However, most CCMs show buffered OH at a global scale (Stevenson et al., 2020), and our comparison between the modelled and observed CO records supports this conclusion.

5.3.2 CO secondary production

If we hypothesize that the past evolution of OH levels is well understood for the period spanning 1920–1980 (Stevenson et al., 2020), CO sources should be investigated to explain the mismatch between modelled and observed CO trends over the time period of 1920–1980: secondary production and/or direct emissions may be involved. Secondary production represents about 50 % of the CO sources in the modern atmosphere (Fig. 1; Szopa et al., 2021) and is largely driven by methane oxidation. The Community Emissions Data System (CEDS) global anthropogenic methane emissions exhibit an 8-fold increase from 1850 to the present (Stevenson et al., 2020), but for all AerChemMIP simulations, atmospheric CH_4 levels are prescribed at the surface based on observations and ice core data (Meinshausen et al., 2017). Thus, atmospheric CH_4 is well constrained, and the CH_4 oxidation CO source is accurately quantified by models. On the other hand, VOC oxidation represents only a small fraction of the modern CO sources ($\sim$ 10 %, Fig. 1; Fortems-Cheiney et al., 2012). AerChemMIP models suggest no large changes in BVOC emissions for the 1850–1980 period (Griffiths et al., 2021). Using the dynamic global vegetation model LPJ-GUESS, Hantson et al. (2017) find that both isoprene and monoterpene, which represent the largest fractions of BVOCs, had higher emissions at the beginning of the 20th century than at present. AerChemMIP models suggest an increase in the growth rate of anthropogenic VOC (AVOC) emissions in the 1950s (Stevenson et al., 2020). However, AVOC oxidation represents a minor source of CO, and an underestimation of the AVOC emissions prior to 1950 is unlikely to explain the differences in modelled and ice archive NH [CO] trends (Fig. 3).

5.3.3 Anthropogenic CO emissions

In the period spanning 1850–1980, the multimodel mean of Arctic [CO] (Fig. 3) evolves with a rate similar to that of its direct emissions in the 30–90° N latitudinal band (Fig. 4). This direct emissions rate is driven by the change in emissions due to fossil fuel combustion, which is itself driven by the changes in emissions from transportation (brown and purple lines in Fig. 4; Hoesly et al., 2018). According to the inventory used in CMIP6, CO biomass burning emissions have exhibited little variation since 1850 (blue line in Fig. 4; van Marle et al., 2017). Prior to 1945, direct anthropogenic CO emissions are largely dominated in magnitude by the RCO sector. In 1945, CO emissions related to transportation started increasing, rapidly dominating other emissions sectors including RCO (Fig. 4). Combustion of fossil fuels is the driver of the trends in CO_2 emissions over the 20th century (see Fig. 2.1, panel A, of the Intergovernmental Panel on Climate Change (IPCC, 2023) synthesis report). CO_2 atmospheric levels are reconstructed thanks to multiple ice core and firn records and have been directly mea-

sured at a growing number of surface stations since 1945. The atmospheric CO_2 record puts a strong constraint on fossil fuel combustion inventories, which can be considered robust. Fossil fuel combustion inventories (also referred as activity datasets) are combined with emission factors (EFs) to estimate atmospheric gas emissions. There is high confidence in emission factors for CO_2, but Hoesly et al. (2018) report that anthropogenic CO EFs prior to 1970 are not well constrained. Combustion EFs for CO are held constant before 1900 at values drawn from a literature review (Winijkul et al., 2016) and are linearly interpolated between 1900 and 1970 by Hoesly et al. (2018). Consequently, we suggest that the mismatch in [CO] trends observed between the AerChemMIP multimodel mean and the ice archive dataset in the NH for the period spanning 1920 to 1980 (Fig. 3) may be related to uncertainties in CO EFs, specifically EFs for the RCO and transportation sectors, which drive the direct CO emission pattern during the 1920–1980 period.

5.4 Biomass burning emissions in the Southern Hemisphere since preindustrial times

The evolution of biomass burning emission inventories since PI times has been recently subject to debate. Biomass burning emission inventories, such as the CMIP6 inventories, commonly scale up fire emissions with population (e.g. van Marle et al., 2017; van der Werf et al., 2013), suggesting lower biomass burning emissions in PI times compared to the present day. On the other hand, hypothesizing a decline in burned areas with increasing population density due to land use changes (Andela et al., 2017; Knorr et al., 2014) leads to biomass burning reaching higher levels in PI times compared to the present day (e.g. Hamilton et al., 2018; Liu et al., 2021; Rowlinson et al., 2020). Notably, Liu et al. (2021) concluded that fire emissions remained relatively stable in the SH between 1750 and $\sim$ 1920, followed by a 30 % decrease until about 1990. These authors support this conclusion by a comparison of simulated black carbon (BC) deposition fluxes and BC measurement conducted on an array of ice cores (14 Antarctic records and 1 record from the Andes).

Our SH [CO] reconstruction from ice archives, as well as the recent SH CO record from Strawson et al. (2024), does not show any decreasing trend in [CO] between 1850 and 1992 (Fig. 2b). Instead, atmospheric CO in the Southern Hemisphere exhibits an increase closely reproduced by AerChemMIP models. If the trend in biomass burning inventories used within the framework of CMIP6 (Fig. 4b) were wrong, as suggested by Liu et al. (2021), this would mean that the trend in anthropogenic CO emissions (Fig. 4) would also be wrong (i.e. underestimated), compensating for an overestimation of fire CO emissions. This seems unlikely.

The Antarctic [CO] reconstructions (Strawson et al., 2024; Faïn et al., 2023a) also disagree with the elevated [CO] levels reported previously by Wang et al. (2010), which concluded that biomass burning CO emissions peaked during the late 19th century at rates roughly 3 times those of modern levels (see Faïn et al., 2023a, for a detailed comparison with the Wang et al. CO dataset). Finally, both models and observations reveal a [CO] growth rate in the SH that is larger by a factor of 2 during the 1945–1980 time period. The modelled trend is mostly driven by an increase in anthropogenic transportation emissions (Fig. 4), and the Antarctic ice archives suggest that such anthropogenic CO emissions are well constrained.

6 Summary and conclusion

We have reported the first bipolar comparison of atmospheric CO mixing ratios extracted from Greenland and Antarctic ice archives to multimodel ACCMIP and AerChemMIP historical ensembles for the period of 1850 to the present. Specifically, the ice archive [CO] records are composites based on multiple ice core and firn air records, with 8 and 10 datasets for Greenland and Antarctica, respectively (Faïn et al., 2023a, 2022a; Petrenko et al., 2013). We used historical CO mixing ratio outputs from the 16 ACCMIP models (Naik et al., 2013) for three time slices (1850, 1980, and 2000) and from 7 models involved in the AerChemMIP exercise (Collins et al., 2017) for the historical period spanning 1850–2014 at an annual resolution.

Both ACCMIP and AerChemMIP model ensembles present negative CO biases at high latitudes, particularly in the Northern Hemisphere, which are still poorly understood and could involve missing anthropogenic emissions, underestimation of the secondary chemical production of CO, or excessive CO losses via OH oxidation. However, the model CO bias at northern high latitudes has decreased by $\sim$ 50 % between the ACCMIP and AerChemMIP exercises.

We used the atmospheric [CO] from the Greenland and Antarctic ice archives as a benchmark for the ACCMIP and AerChemMIP ensembles to assess both the global chemistry–climate models and the emission datasets they used. Over the period of 1980–2010, CO trends from ice archives and AerChemMIP multimodel outputs are in excellent agreement at both the northern and southern high latitudes. Such agreement suggests that the trends in surface emissions of CO (including anthropogenic emissions), as well as in the main CO sink (OH oxidation), are now accurately represented within models.

Over the 1920 to 1980 period, a mismatch in [CO] trends remains between the AerChemMIP multimodel mean and the ice archive dataset in the NH, with the multimodel mean showing a lower trend before 1945 and a higher trend after 1945. Although the Greenland ice archive record should only be considered an upper bound of the past CO abundance, as we cannot fully rule out in situ production artifacts (Faïn et al., 2022a), we suggest that the mismatch between modelled and observed CO trends at NH high latitudes is related to uncertainties in anthropogenic CO emission fac-

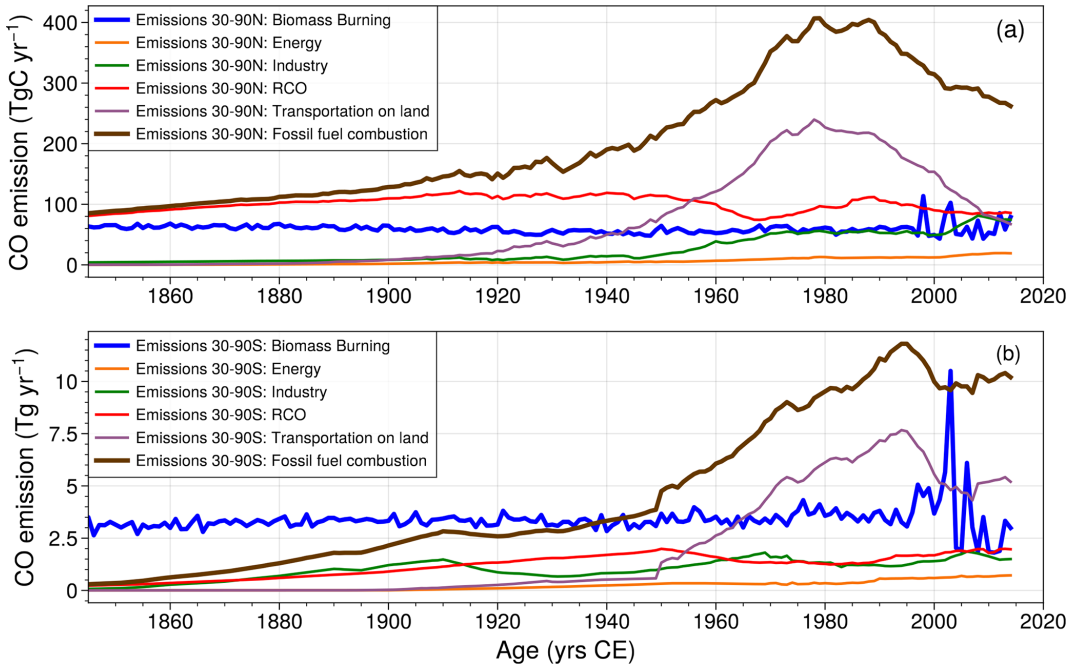

Figure 4. CEDS anthropogenic emission estimates for the 30–90° N **(a)** and 30–90° S **(b)** latitudinal bands by aggregate sectors (Hoesly et al., 2018): energy, industry, RCO, and transportation. "RCO" stands for residential, commercial, and other. "Fossil fuel combustion" combines all sectors listed before and small contributions from the waste and shipping sectors (grouped together). Biomass burning emissions from the 30–90° latitudinal bands are from van Marle et al. (2017).

tors, specifically EFs for the residential, commercial, and other and transportation sectors. Our study indicates that a better evaluation of these EFs would be an area of improvement for the modelling of the past NH [CO]. Finally, SH atmospheric [CO] exhibits an increase closely reproduced by AerChemMIP models, supporting the biomass burning inventories used within the framework of CMIP6 (van Marle et al., 2017). The hypothesis of higher fire emissions at the onset of the 20th century (e.g. Liu et al., 2021) seems unlikely in the light of our results and those of Strawson et al. (2024), who used box modelling to reconstruct historical fire emissions.

Although imperfect, state-of-the-art global chemistry–climate models are now better able to represent trends in atmospheric [CO] at high latitudes. Further modelling sensitivity studies would provide a better understanding of the nature of the CO bias at NH high latitudes, and this study shows that CO trends from ice cores can now serve as a constraint to better disentangle the causes of CO bias. Also, isotopic information can help to determine the various CO sources and their relative magnitudes (e.g. Röckmann et al., 2002). Including isotope data in modelling atmospheric chemistry schemes has been shown to help constrain source strengths of CO (Park et al., 2015). Thus, more measurements of the stable isotopes of CO from firn and ice cores would help constrain relative CO source strengths in the past. This work offers a new constraint to better characterize emissions factors over the past century and thus could contribute to a revision of past tropospheric ozone or methane lifetime evolutions. On the other hand, a recent record from Strawson et al. (2024) suggests that atmospheric SH [CO] may have experienced greater trend variability than predicted by state-of-the-art chemistry–climate models, suggesting that historical CO dynamics have not been fully accounted for. Improvement in the assessment of past OH trends (e.g. using innovative proxies such as ^{14}CO; Brenninkmeijer et al., 2022) would also provide powerful constraints on the past evolution of the main CO sink.

Data availability. The Antarctic ice archive [CO] reconstructions and the atmospheric [CO] from Mawson Station (Antarctica) are accessible on PANGEAE: https://doi.org/10.1594/PANGAEA.960615 (Faïn et al., 2023b). The Greenland ice core [CO] record is also accessible on https://doi.org/10.1594/PANGAEA.941919 (Faïn et al., 2022b). ACCMIP model outputs are available at the Comprehensive Environmental Data Archive dataset repository (http://catalogue.ceda.ac.uk/uuid/ded523bf23d59910e5d73f1703a2d540/, Shindell et al., 2011, Sect. 3.2). AerChemMip model outputs are available at the ESGF dataset repository (https://aims2.llnl.gov/search, Earth System Grid Federation, 2024, Sect. 4.2).

Supplement. The supplement related to this article is available online at: https://doi.org/10.5194/acp-25-1105-2025-supplement.

Author contributions. This scientific project was designed by XF and SS, with major contributions from DME, VVP, and RHR. Carbon monoxide measurements were carried out by XF, RHR, KF, DME, and PP. Firn air CO records were modelled by PM and CMT. All authors contributed to data interpretation, with specific input on the interpretation of CMIP5 and CMIP6 results from SS and VN. The paper was written by XF, with the help of all co-authors.

Competing interests. The contact author has declared that none of the authors has any competing interests.

Disclaimer. Publisher's note: Copernicus Publications remains neutral with regard to jurisdictional claims made in the text, published maps, institutional affiliations, or any other geographical representation in this paper. While Copernicus Publications makes every effort to include appropriate place names, the final responsibility lies with the authors.

Acknowledgements. The authors would like to thank all the drillers, field crews, and scientists who participated in the collection, analysis, and interpretation of ice core and firn air samples for CO and who helped produce the CO dataset included in this study. We acknowledge the World Climate Research Programme, which, through its working group on coupled modelling, coordinated and promoted AerChemMIP, a CMIP6-endorsed modelling intercomparison project. We thank the climate modelling centres for producing and making available their model output, the Earth System Grid Federation (ESGF) for archiving the data and providing access, and the multiple funding agencies who supported CMIP6 and ESGF. We are also grateful to ACCMIP, an IGAC project under the International Geosphere–Biosphere Project (IGBP) and World Climate Research Program (WCRP), and the British Atmospheric Data Centre (BADC), which is part of the NERC National Centre for Atmospheric Science (NCAS), for collecting and archiving the ACCMIP data. We thank the three anonymous reviewers for their careful reading of our paper and their many insightful comments and suggestions.

Financial support. This work has been supported by the French ANR (grant no. 10-RPDOC-002-01, project "RPD-COCLICO"; Xavier Faïn), the French national programme LEFE/INSU (project "GreenCO"; Xavier Faïn), the EU FP7-IP (grant no. ENV-2010/265148, project "Pegasos"; Xavier Faïn), and the FP7 ERC (grant no. 291062, project "Ice and Lasers"; Jérôme Chappellaz). Rachael H. Rhodes has received funding from the Isaac Newton Trust (grant no. LBZG/080). Kévin Fourteau's current position is funded by the European Research Council (ERC) under the European Union's Horizon 2020 research and innovation programme ("IVORI"; grant no. 949516).

Review statement. This paper was edited by Sergio Rodríguez and reviewed by three anonymous referees.

References

Andela, N., Morton, D. C., Giglio, L., Chen, Y., van der Werf, G. R., Kasibhatla, P. S., DeFries, R. S., Collatz, G. J., Hantson, S., Kloster, S., Bachelet, D., Forrest, M., Lasslop, G., Li, F., Mangeon, S., Melton, J. R., Yue, C., and Randerson, J. T.: A human-driven decline in global burned area, Science, 356, 1356–1362, https://doi.org/10.1126/science.aal4108, 2017.

Archibald, A. T., O'Connor, F. M., Abraham, N. L., Archer-Nicholls, S., Chipperfield, M. P., Dalvi, M., Folberth, G. A., Dennison, F., Dhomse, S. S., Griffiths, P. T., Hardacre, C., Hewitt, A. J., Hill, R. S., Johnson, C. E., Keeble, J., Köhler, M. O., Morgenstern, O., Mulcahy, J. P., Ordóñez, C., Pope, R. J., Rumbold, S. T., Russo, M. R., Savage, N. H., Sellar, A., Stringer, M., Turnock, S. T., Wild, O., and Zeng, G.: Description and evaluation of the UKCA stratosphere–troposphere chemistry scheme (StratTrop vn 1.0) implemented in UKESM1, Geosci. Model Dev., 13, 1223–1266, https://doi.org/10.5194/gmd-13-1223-2020, 2020.

Bauer, S. E., Tsigaridis, K., Faluvegi, G., Kelley, M., Lo, K. K., Miller, R. L., Nazarenko, L., Schmidt, G. A., and Wu, J.: Historical (1850–2014) Aerosol Evolution and Role on Climate Forcing Using the GISS ModelE2.1 Contribution to CMIP6, J. Adv. Model. Earth Sy., 12, e2019MS001978, https://doi.org/10.1029/2019MS001978, 2020.

Brenninkmeijer, C. A. M., Gromov, S. S., and Jöckel, P.: Cosmogenic ^{14}CO for assessing the oh-based self-cleaning capacity of the troposphere, Radiocarbon, 64, 761–779, https://doi.org/10.1017/RDC.2021.101, 2022.

Bruhn, D., Albert, K. R., Mikkelsen, T. N., and Ambus, P.: UV-induced carbon monoxide emission from living vegetation, Biogeosciences, 10, 7877–7882, https://doi.org/10.5194/bg-10-7877-2013, 2013.

Buchholz, R. R., Worden, H. M., Park, M., Francis, G., Deeter, M. N., Edwards, D. P., Emmons, L. K., Gaubert, B., Gille, J., Martínez-Alonso, S., Tang, W., Kumar, R., Drummond, J. R., Clerbaux, C., George, M., Coheur, P.-F., Hurtmans, D., Bowman, K. W., Luo, M., Payne, V. H., Worden, J. R., Chin, M., Levy, R. C., Warner, J., Wei, Z., and Kulawik, S. S.: Air pollution trends measured from Terra: CO and AOD over industrial, fire-prone, and background regions, Remote Sens. Environ., 256, 112275, https://doi.org/10.1016/J.RSE.2020.112275, 2021.

Collins, W. J., Lamarque, J.-F., Schulz, M., Boucher, O., Eyring, V., Hegglin, M. I., Maycock, A., Myhre, G., Prather, M., Shindell, D., and Smith, S. J.: AerChemMIP: quantifying the effects of chemistry and aerosols in CMIP6, Geosci. Model Dev., 10, 585–607, https://doi.org/10.5194/gmd-10-585-2017, 2017.

Conte, L., Szopa, S., Séférian, R., and Bopp, L.: The oceanic cycle of carbon monoxide and its emissions to the atmosphere, Biogeosciences, 16, 881–902, https://doi.org/10.5194/bg-16-881-2019, 2019.

Crutzen, P. J.: A discussion of the chemistry of some minor constituents in the stratosphere and troposphere, Pure Appl. Geophys., 106–108, 1385–1399, https://doi.org/10.1007/BF00881092, 1973.

Duncan, B. N., Logan, J. A., Bey, I., Megretskaia, I. A., Yantosca, R. M., Novelli, P. C., Jones, N. B., and Rinsland, C. P.: Global budget of CO, 1988–1997: Source estimates and validation with a global model, J. Geophys. Res.-Atmos., 112, D22301, https://doi.org/10.1029/2007jd008459, 2007.

Dunne, J. P., Horowitz, L. W., Adcroft, A. J., Ginoux, P., Held, I. M., John, J. G., Krasting, J. P., Malyshev, S., Naik, V., Paulot, F., Shevliakova, E., Stock, C. A., Zadeh, N., Balaji, V., Blanton, C., Dunne, K. A., Dupuis, C., Durachta, J., Dussin, R., Gauthier, P. P. G., Griffies, S. M., Guo, H., Hallberg, R. W., Harrison, M., He, J., Hurlin, W., McHugh, C., Menzel, R., Milly, P. C. D., Nikonov, S., Paynter, D. J., Ploshay, J., Radhakrishnan, A., Rand, K., Reichl, B. G., Robinson, T., Schwarzkopf, D. M., Sentman, L. T., Underwood, S., Vahlenkamp, H., Winton, M., Wittenberg, A. T., Wyman, B., Zeng, Y., and Zhao, M.: The GFDL Earth System Model Version 4.1 (GFDL-ESM 4.1): Overall Coupled Model Description and Simulation Characteristics, J. Adv. Model. Earth Sy., 12, e2019MS002015, https://doi.org/10.1029/2019MS002015, 2020.

Earth System Grid Federation: https://aims2.llnl.gov/search, last access: July 2024.

Emmons, L. K., Schwantes, R. H., Orlando, J. J., Tyndall, G., Kinnison, D., Lamarque, J.-F., Marsh, D., Mills, M. J., Tilmes, S., Bardeen, C., Buchholz, R. R., Conley, A., Gettelman, A., Garcia, R., Simpson, I., Blake, D. R., Meinardi, S., and Pétron, G.: The Chemistry Mechanism in the Community Earth System Model Version 2 (CESM2), J. Adv. Model. Earth Sy., 12, e2019MS001882, https://doi.org/10.1029/2019MS001882, 2020.

Faïn, X., Chappellaz, J., Rhodes, R. H., Stowasser, C., Blunier, T., McConnell, J. R., Brook, E. J., Preunkert, S., Legrand, M., Debois, T., and Romanini, D.: High resolution measurements of carbon monoxide along a late Holocene Greenland ice core: evidence for in situ production, Clim. Past, 10, 987–1000, https://doi.org/10.5194/cp-10-987-2014, 2014.

Faïn, X., Rhodes, R. H., Place, P., Petrenko, V. V., Fourteau, K., Chellman, N., Crosier, E., McConnell, J. R., Brook, E. J., Blunier, T., Legrand, M., and Chappellaz, J.: Northern Hemisphere atmospheric history of carbon monoxide since preindustrial times reconstructed from multiple Greenland ice cores, Clim. Past, 18, 631–647, https://doi.org/10.5194/cp-18-631-2022, 2022a.

Faïn, X., Rhodes, R. H, Place, P., Petrenko, V. V., Fourteau, K., Chellman, N. J., Crosier, E., McConnell, J. R., Brook, E. J., Blunier, T., Legrand, M., Chappellaz, J. A.: Multisite composite atmospheric Arctic CO record, PANGAEA [dataset], https://doi.org/10.1594/PANGAEA.941919, in: Faïn, X. et al. (2022): High resolution, continous, carbon monoxide records from Greenland ice cores [dataset bundled publication], PANGAEA, https://doi.org/10.1594/PANGAEA.941920, 2022b.

Faïn, X., Etheridge, D. M., Fourteau, K., Martinerie, P., Trudinger, C. M., Rhodes, R. H., Chellman, N. J., Langenfelds, R. L., McConnell, J. R., Curran, M. A. J., Brook, E. J., Blunier, T., Teste, G., Grilli, R., Lemoine, A., Sturges, W. T., Vannière, B., Freitag, J., and Chappellaz, J.: Southern Hemisphere atmospheric history of carbon monoxide over the late Holocene reconstructed from multiple Antarctic ice archives, Clim. Past, 19, 2287–2311, https://doi.org/10.5194/cp-19-2287-2023, 2023a.

Faïn, X., Etherdige, D. M., Fourteau, K., Martinerie, P., Trudinger, C. M., Rhodes, R. H., Chellman, N. J., Langenfelds, R. L., McConnell, J. R., Curran, M., Brook, E. J., Blunier, T., Teste, G., Grilli, R., Anthony, L., Sturges, W. T., Vannière, B., Freitag, J., and Jérôme, C.: Carbon monoxide (CO) Antarctic records from ice cores (DC12, ABN, Taldice), firn air (DE08-2, DSSW19K, DSSW20K, South Pole, ABN, Lock-In), and Mawson Station atmospheric history from -835 to 2021 CE [dataset bundled publication], PANGAEA, https://doi.org/10.1594/PANGAEA.960615, 2023b.

Feng, L., Smith, S. J., Braun, C., Crippa, M., Gidden, M. J., Hoesly, R., Klimont, Z., van Marle, M., van den Berg, M., and van der Werf, G. R.: The generation of gridded emissions data for CMIP6, Geosci. Model Dev., 13, 461–482, https://doi.org/10.5194/gmd-13-461-2020, 2020.

Fortems-Cheiney, A., Chevallier, F., Pison, I., Bousquet, P., Saunois, M., Szopa, S., Cressot, C., Kurosu, T. P., Chance, K., and Fried, A.: The formaldehyde budget as seen by a global-scale multi-constraint and multi-species inversion system, Atmos. Chem. Phys., 12, 6699–6721, https://doi.org/10.5194/acp-12-6699-2012, 2012.

Gaubert, B., Worden, H. M., Arellano, A. F. J., Emmons, L. K., Tilmes, S., Barré, J., Martinez Alonso, S., Vitt, F., Anderson, J. L., Alkemade, F., Houweling, S., and Edwards, D. P.: Chemical feedback from decreasing carbon monoxide emissions, Geophys. Res. Lett., 44, 9985–9995, https://doi.org/10.1002/2017GL074987, 2017.

Gaubert, B., Emmons, L. K., Raeder, K., Tilmes, S., Miyazaki, K., Arellano Jr., A. F., Elguindi, N., Granier, C., Tang, W., Barré, J., Worden, H. M., Buchholz, R. R., Edwards, D. P., Franke, P., Anderson, J. L., Saunois, M., Schroeder, J., Woo, J.-H., Simpson, I. J., Blake, D. R., Meinardi, S., Wennberg, P. O., Crounse, J., Teng, A., Kim, M., Dickerson, R. R., He, H., Ren, X., Pusede, S. E., and Diskin, G. S.: Correcting model biases of CO in East Asia: impact on oxidant distributions during KORUS-AQ, Atmos. Chem. Phys., 20, 14617–14647, https://doi.org/10.5194/acp-20-14617-2020, 2020.

Griffiths, P. T., Murray, L. T., Zeng, G., Shin, Y. M., Abraham, N. L., Archibald, A. T., Deushi, M., Emmons, L. K., Galbally, I. E., Hassler, B., Horowitz, L. W., Keeble, J., Liu, J., Moeini, O., Naik, V., O'Connor, F. M., Oshima, N., Tarasick, D., Tilmes, S., Turnock, S. T., Wild, O., Young, P. J., and Zanis, P.: Tropospheric ozone in CMIP6 simulations, Atmos. Chem. Phys., 21, 4187–4218, https://doi.org/10.5194/acp-21-4187-2021, 2021.

Guenther, A., Karl, T., Harley, P., Wiedinmyer, C., Palmer, P. I., and Geron, C.: Estimates of global terrestrial isoprene emissions using MEGAN (Model of Emissions of Gases and Aerosols from Nature), Atmos. Chem. Phys., 6, 3181–3210, https://doi.org/10.5194/acp-6-3181-2006, 2006.

Haan, D. and Raynaud, D.: Ice core record of CO variations during the last two millennia: atmospheric implications and chemical interactions within the Greenland ice, Tellus B, 50, 253–262, 1998.

Haan, D., Martinerie, P., and Raynaud, D.: Ice core data of atmospheric carbon monoxide over Antarctica and Greenland during the last 200 years, Geophys. Res. Lett., 23, 2235–2238, 1996.

Hamilton, D. S., Hantson, S., Scott, C. E., Kaplan, J. O., Pringle, K. J., Nieradzik, L. P., Rap, A., Folberth, G. A., Spracklen, D. V., and Carslaw, K. S.: Reassessment of pre-industrial fire emissions strongly affects anthropogenic aerosol forcing, Nat. Commun., 9, 3182, https://doi.org/10.1038/s41467-018-05592-9, 2018.

Hantson, S., Knorr, W., Schurgers, G., Pugh, T. A. M., and Arneth, A.: Global isoprene and monoterpene emissions under changing climate, vegetation, CO_2 and land use, Atmos. Environ., 155, 35–45, https://doi.org/10.1016/j.atmosenv.2017.02.010, 2017.

Heimann, I., Griffiths, P. T., Warwick, N. J., Abraham, N. L., Archibald, A. T., and Pyle, J. A.: Methane Emissions in a Chemistry-Climate Model: Feedbacks and Climate Response, J. Adv. Model. Earth Sy., 12, e2019MS002019, https://doi.org/10.1029/2019MS002019, 2020.

Hoesly, R. M., Smith, S. J., Feng, L., Klimont, Z., Janssens-Maenhout, G., Pitkanen, T., Seibert, J. J., Vu, L., Andres, R. J., Bolt, R. M., Bond, T. C., Dawidowski, L., Kholod, N., Kurokawa, J.-I., Li, M., Liu, L., Lu, Z., Moura, M. C. P., O'Rourke, P. R., and Zhang, Q.: Historical (1750–2014) anthropogenic emissions of reactive gases and aerosols from the Community Emissions Data System (CEDS), Geosci. Model Dev., 11, 369–408, https://doi.org/10.5194/gmd-11-369-2018, 2018.

Horowitz, L. W., Naik, V., Paulot, F., Ginoux, P. A., Dunne, J. P., Mao, J., Schnell, J., Chen, X., He, J., John, J. G., Lin, M., Lin, P., Malyshev, S., Paynter, D., Shevliakova, E., and Zhao, M.: The GFDL Global Atmospheric Chemistry-Climate Model AM4.1: Model Description and Simulation Characteristics, J. Adv. Model. Earth Sy., 12, e2019MS002032, https://doi.org/10.1029/2019MS002032, 2020.

IPCC: in: Climate Change 2023: Synthesis Report. Contribution of Working Groups I, II and III to the Sixth Assessment Report of the Intergovernmental Panel on Climate Change, edited by: Core Writing Team, Lee, H., and Romero, J., IPCC, Geneva, Switzerland, 35–115, https://doi.org/10.59327/IPCC/AR6-9789291691647, 2023.

Khalil, M. A. K., Pinto, J. P., and Shearer, M. J.: Atmospheric carbon monoxide, Chemosphere – Glob. Change Sci., 1, ix–xi, https://doi.org/10.1016/S1465-9972(99)00053-7, 1999.

Knorr, W., Kaminski, T., Arneth, A., and Weber, U.: Impact of human population density on fire frequency at the global scale, Biogeosciences, 11, 1085–1102, https://doi.org/10.5194/bg-11-1085-2014, 2014.

Lamarque, J.-F., Bond, T. C., Eyring, V., Granier, C., Heil, A., Klimont, Z., Lee, D., Liousse, C., Mieville, A., Owen, B., Schultz, M. G., Shindell, D., Smith, S. J., Stehfest, E., Van Aardenne, J., Cooper, O. R., Kainuma, M., Mahowald, N., McConnell, J. R., Naik, V., Riahi, K., and van Vuuren, D. P.: Historical (1850–2000) gridded anthropogenic and biomass burning emissions of reactive gases and aerosols: methodology and application, Atmos. Chem. Phys., 10, 7017–7039, https://doi.org/10.5194/acp-10-7017-2010, 2010.

Lamarque, J.-F., Shindell, D. T., Josse, B., Young, P. J., Cionni, I., Eyring, V., Bergmann, D., Cameron-Smith, P., Collins, W. J., Doherty, R., Dalsoren, S., Faluvegi, G., Folberth, G., Ghan, S. J., Horowitz, L. W., Lee, Y. H., MacKenzie, I. A., Nagashima, T., Naik, V., Plummer, D., Righi, M., Rumbold, S. T., Schulz, M., Skeie, R. B., Stevenson, D. S., Strode, S., Sudo, K., Szopa, S., Voulgarakis, A., and Zeng, G.: The Atmospheric Chemistry and Climate Model Intercomparison Project (ACCMIP): overview and description of models, simulations and climate diagnostics, Geosci. Model Dev., 6, 179–206, https://doi.org/10.5194/gmd-6-179-2013, 2013.

Liu, P., Kaplan, J. O., Mickley, L. J., Li, Y., Chellman, N. J., Arienzo, M. M., Kodros, J. K., Pierce, J. R., Sigl, M., Freitag, J., Mulvaney, R., Curran, M. A. J., and McConnell, J. R.: Improved estimates of preindustrial biomass burning reduce the magnitude of aerosol climate forcing in the Southern Hemisphere, Sci. Adv. 7, eabc1379, 2021.

Loh, Z., Langenfelds, R. L., and Krummel, P. B.: Atmospheric CO at Mawson by Commonwealth Scientific and Industrial Research Organisation, CO_MAA_surfaceflask_CSIRO_data1, WDCGG [data set], ver.2021-04-08-1004, https://gaw.kishou.go.jp/search/file/0016-7005-3001-01-02-9999 (last access: March 2023), 2021.

Meinshausen, M., Vogel, E., Nauels, A., Lorbacher, K., Meinshausen, N., Etheridge, D. M., Fraser, P. J., Montzka, S. A., Rayner, P. J., Trudinger, C. M., Krummel, P. B., Beyerle, U., Canadell, J. G., Daniel, J. S., Enting, I. G., Law, R. M., Lunder, C. R., O'Doherty, S., Prinn, R. G., Reimann, S., Rubino, M., Velders, G. J. M., Vollmer, M. K., Wang, R. H. J., and Weiss, R.: Historical greenhouse gas concentrations for climate modelling (CMIP6), Geosci. Model Dev., 10, 2057–2116, https://doi.org/10.5194/gmd-10-2057-2017, 2017.

Miyazaki, K., Bowman, K. W., Yumimoto, K., Walker, T., and Sudo, K.: Evaluation of a multi-model, multi-constituent assimilation framework for tropospheric chemical reanalysis, Atmos. Chem. Phys., 20, 931–967, https://doi.org/10.5194/acp-20-931-2020, 2020.

Naik, V., Voulgarakis, A., Fiore, A. M., Horowitz, L. W., Lamarque, J.-F., Lin, M., Prather, M. J., Young, P. J., Bergmann, D., Cameron-Smith, P. J., Cionni, I., Collins, W. J., Dalsøren, S. B., Doherty, R., Eyring, V., Faluvegi, G., Folberth, G. A., Josse, B., Lee, Y. H., MacKenzie, I. A., Nagashima, T., van Noije, T. P. C., Plummer, D. A., Righi, M., Rumbold, S. T., Skeie, R., Shindell, D. T., Stevenson, D. S., Strode, S., Sudo, K., Szopa, S., and Zeng, G.: Preindustrial to present-day changes in tropospheric hydroxyl radical and methane lifetime from the Atmospheric Chemistry and Climate Model Intercomparison Project (ACCMIP), Atmos. Chem. Phys., 13, 5277–5298, https://doi.org/10.5194/acp-13-5277-2013, 2013.

Oshima, N., Yukimoto, S., Deushi, M., Koshiro, T., Kawai, H., Tanaka, T. Y., and Yoshida, K.: Global and Arctic effective radiative forcing of anthropogenic gases and aerosols in MRI-ESM2.0, Prog. Earth Planet Sci., 7, 38, https://doi.org/10.1186/s40645-020-00348-w, 2020.

Pacifico, F., Harrison, S. P., Jones, C. D., Arneth, A., Sitch, S., Weedon, G. P., Barkley, M. P., Palmer, P. I., Serça, D., Potosnak, M., Fu, T.-M., Goldstein, A., Bai, J., and Schurgers, G.: Evaluation of a photosynthesis-based biogenic isoprene emission scheme in JULES and simulation of isoprene emissions under present-day climate conditions, Atmos. Chem. Phys., 11, 4371–4389, https://doi.org/10.5194/acp-11-4371-2011, 2011.

Park, K., Wang, Z., Emmons, L. K., and Mak, J. E.: Variation of atmospheric CO, $\delta^{13}C$, and $\delta^{18}O$ at high northern latitude during 2004–2009: Observations and model simulations, J. Geophys. Res.-Atmos., 120, 11024–11036, https://doi.org/10.1002/2015JD023191, 2015.

Petrenko, V. V., Martinerie, P., Novelli, P., Etheridge, D. M., Levin, I., Wang, Z., Blunier, T., Chappellaz, J., Kaiser, J., Lang, P., Steele, L. P., Hammer, S., Mak, J., Langenfelds, R. L., Schwander, J., Severinghaus, J. P., Witrant, E., Petron, G., Battle, M. O., Forster, G., Sturges, W. T., Lamarque, J.-F., Steffen, K., and White, J. W. C.: A 60 yr record of atmospheric carbon monoxide reconstructed from Greenland firn air, Atmos. Chem. Phys., 13, 7567–7585, https://doi.org/10.5194/acp-13-7567-2013, 2013.

Petron, G., Crotwell, A. M., Dlugokencky, E. J., Madronich, M., Moglia, E., Neff, D., Thoning, K., Wolter, S., and

Mund, J. W.: Atmospheric Carbon Monoxide Dry Air Mole Fractions from the NOAA GML Carbon Cycle Cooperative Global Air Sampling Network, 1988–2022, Version: 2023-08-28, https://doi.org/10.15138/33bv-s284, 2023.

Röckmann, T., Jöckel, P., Gros, V., Bräunlich, M., Possnert, G., and Brenninkmeijer, C. A. M.: Using ^{14}C, ^{13}C, ^{18}O and ^{17}O isotopic variations to provide insights into the high northern latitude surface CO inventory, Atmos. Chem. Phys., 2, 147–159, https://doi.org/10.5194/acp-2-147-2002, 2002.

Rowlinson, M. J., Rap, A., Hamilton, D. S., Pope, R. J., Hantson, S., Arnold, S. R., Kaplan, J. O., Arneth, A., Chipperfield, M. P., Forster, P. M., and Nieradzik, L.: Tropospheric ozone radiative forcing uncertainty due to pre-industrial fire and biogenic emissions, Atmos. Chem. Phys., 20, 10937–10951, https://doi.org/10.5194/acp-20-10937-2020, 2020.

Schultz, M. G., Akimoto, H., Bottenheim, J., Buchmann, B., Galbally, I. E., Gilge, S., Helmig, D., Koide, H., Lewis, A. C., Novelli, P. C., Plass-Dölmer, C., Ryerson, T. B., Steinbacher, M., Steinbrecher, R., Tarasova, O., Tørseth, K., Thouret, V., and Zellweger, C.: The global atmosphere watch reactive gases measurement network, Elementa, 3, 1–23, 2015.

Shindell, D. T., Faluvegi, G., Stevenson, D. S., Krol, M. C., Emmons, L. K., Lamarque, J.-F., Pétron, G., Dentener, F. J., Ellingsen, K., Schultz, M. G., Wild, O., Amann, M., Atherton, C. S., Bergmann, D. J., Bey, I., Butler, T., Cofala, J., Collins, W. J., Derwent, R. G., Doherty, R. M., Drevet, J., Eskes, H. J., Fiore, A. M., Gauss, M., Hauglustaine, D. A., Horowitz, L. W., Isaksen, I. S. A., Lawrence, M. G., Montanaro, V., Müller, J.-F., Pitari, G., Prather, M. J., Pyle, J. A., Rast, S., Rodriguez, J. M., Sanderson, M. G., Savage, N. H., Strahan, S. E., Sudo, K., Szopa, S., Unger, N., van Noije, T. P. C., and Zeng, G.: Multimodel simulations of carbon monoxide: Comparison with observations and projected near-future changes, J. Geophys. Res., 111, D19306, https://doi.org/10.1029/2006JD007100, 2006.

Shindell, D., Lamarque, J. F., Collins, W., Eyring, V., Nagashima, T., Naik, V., Szopa, S., and Zeng, G.: The model data outputs from the Atmospheric Chemistry & Climate Model Intercomparison Project (ACCMIP), NERC EDS Centre for Environmental Data Analysis [data set], http://catalogue.ceda.ac.uk/uuid/ded523bf23d59910e5d73f1703a2d540/ (last access: August 2021), 2011.

Stein, O., Schultz, M. G., Bouarar, I., Clark, H., Huijnen, V., Gaudel, A., George, M., and Clerbaux, C.: On the wintertime low bias of Northern Hemisphere carbon monoxide found in global model simulations, Atmos. Chem. Phys., 14, 9295–9316, https://doi.org/10.5194/acp-14-9295-2014, 2014.

Stevenson, D. S., Zhao, A., Naik, V., O'Connor, F. M., Tilmes, S., Zeng, G., Murray, L. T., Collins, W. J., Griffiths, P. T., Shim, S., Horowitz, L. W., Sentman, L. T., and Emmons, L.: Trends in global tropospheric hydroxyl radical and methane lifetime since 1850 from AerChemMIP, Atmos. Chem. Phys., 20, 12905–12920, https://doi.org/10.5194/acp-20-12905-2020, 2020.

Strawson, I., Faïn, X., Bauska, T. K., Muschitiello, F., Vladimirova, D. O., Tetzner, D. R., Humby, J., Thomas, E. R., Liu, P., Zhang, B., Grilli, R., and Rhodes, R. H.: Historical Southern Hemisphere biomass burning variability inferred from ice core carbon monoxide records, P. Natl. Acad. Sci. USA, 121, e2402868121, https://doi.org/10.1073/pnas.2402868121, 2024.

Strode, S. A., Duncan, B. N., Yegorova, E. A., Kouatchou, J., Ziemke, J. R., and Douglass, A. R.: Implications of carbon monoxide bias for methane lifetime and atmospheric composition in chemistry climate models, Atmos. Chem. Phys., 15, 11789–11805, https://doi.org/10.5194/acp-15-11789-2015, 2015.

Szopa, S., Naïk, V., Adhikary, B., Artaxo, P., Berntsen, T., Collins, W. D., Fuzzi, S., Gallardo, L., Kiendler-Scharr, A., Klimont, Z., Liao, H., Unger, N., and Zanis, P.: Climate Change 2021 – The Physical Science Basis. Contribution of Working Group I to the Sixth Assessment Report of the Intergovernmental Panel on Climate Change, 1st edn., edited by: Masson-Delmotte, V., Zhai, P., Pirani, A., Connors, S. L., Péan, C., Berger, S., Caud, N., Chen, Y., Goldfarb, L., Gomis, M. I., Huang, M., Leitzell, K., Lonnoy, E., Matthews, J. B. R., Maycock, T. K., Waterfield, T., Yelekçi, O., Yu, R., and Zhou, B., Cambridge University Press, Cambridge, United Kingdom and New York, NY, USA, 817–922, https://doi.org/10.1017/9781009157896.008, 2021.

van der Werf, G. R., Peters, W., van Leeuwen, T. T., and Giglio, L.: What could have caused pre-industrial biomass burning emissions to exceed current rates?, Clim. Past, 9, 289–306, https://doi.org/10.5194/cp-9-289-2013, 2013.

van der Werf, G. R., Randerson, J. T., Giglio, L., van Leeuwen, T. T., Chen, Y., Rogers, B. M., Mu, M., van Marle, M. J. E., Morton, D. C., Collatz, G. J., Yokelson, R. J., and Kasibhatla, P. S.: Global fire emissions estimates during 1997–2016, Earth Syst. Sci. Data, 9, 697–720, https://doi.org/10.5194/essd-9-697-2017, 2017.

van Marle, M. J. E., Kloster, S., Magi, B. I., Marlon, J. R., Daniau, A.-L., Field, R. D., Arneth, A., Forrest, M., Hantson, S., Kehrwald, N. M., Knorr, W., Lasslop, G., Li, F., Mangeon, S., Yue, C., Kaiser, J. W., and van der Werf, G. R.: Historic global biomass burning emissions for CMIP6 (BB4CMIP) based on merging satellite observations with proxies and fire models (1750–2015), Geosci. Model Dev., 10, 3329–3357, https://doi.org/10.5194/gmd-10-3329-2017, 2017.

van Noije, T., Bergman, T., Le Sager, P., O'Donnell, D., Makkonen, R., Gonçalves-Ageitos, M., Döscher, R., Fladrich, U., von Hardenberg, J., Keskinen, J.-P., Korhonen, H., Laakso, A., Myriokefalitakis, S., Ollinaho, P., Pérez García-Pando, C., Reerink, T., Schrödner, R., Wyser, K., and Yang, S.: EC-Earth3-AerChem: a global climate model with interactive aerosols and atmospheric chemistry participating in CMIP6, Geosci. Model Dev., 14, 5637–5668, https://doi.org/10.5194/gmd-14-5637-2021, 2021.

Wang, Z., Chappellaz, J., Park, J. Y., and Mak, J.: Large variations in Southern Hemisphere biomass burning during the last 650 years, Science, 330, 1663–1666, https://doi.org/10.1126/science.1197257, 2010.

Wang, Z., Chappellaz, J., Martinerie, P., Park, K., Petrenko, V., Witrant, E., Emmons, L. K., Blunier, T., Brenninkmeijer, C. A. M., and Mak, J. E.: The isotopic record of Northern Hemisphere atmospheric carbon monoxide since 1950: implications for the CO budget, Atmos. Chem. Phys., 12, 4365–4377, https://doi.org/10.5194/acp-12-4365-2012, 2012.

Wild, O., Voulgarakis, A., O'Connor, F., Lamarque, J.-F., Ryan, E. M., and Lee, L.: Global sensitivity analysis of chemistry–climate model budgets of tropospheric ozone and OH: exploring model diversity, Atmos. Chem. Phys., 20, 4047–4058, https://doi.org/10.5194/acp-20-4047-2020, 2020.

Winijkul, E., Fierce, L., and Bond, T. C.: Emissions from residential combustion considering end-uses and spatial constraints: Part I, methods and spatial distribution, Atmos. Environ., 125, 126–139, https://doi.org/10.1016/j.atmosenv.2015.10.013, 2016.

Wu, T., Zhang, F., Zhang, J., Jie, W., Zhang, Y., Wu, F., Li, L., Yan, J., Liu, X., Lu, X., Tan, H., Zhang, L., Wang, J., and Hu, A.: Beijing Climate Center Earth System Model version 1 (BCC-ESM1): model description and evaluation of aerosol simulations, Geosci. Model Dev., 13, 977–1005, https://doi.org/10.5194/gmd-13-977-2020, 2020.

Young, P. J., Archibald, A. T., Bowman, K. W., Lamarque, J.-F., Naik, V., Stevenson, D. S., Tilmes, S., Voulgarakis, A., Wild, O., Bergmann, D., Cameron-Smith, P., Cionni, I., Collins, W. J., Dalsøren, S. B., Doherty, R. M., Eyring, V., Faluvegi, G., Horowitz, L. W., Josse, B., Lee, Y. H., MacKenzie, I. A., Nagashima, T., Plummer, D. A., Righi, M., Rumbold, S. T., Skeie, R. B., Shindell, D. T., Strode, S. A., Sudo, K., Szopa, S., and Zeng, G.: Preindustrial to end 21st century projections of tropospheric ozone from the Atmospheric Chemistry and Climate Model Intercomparison Project (ACCMIP), Atmos. Chem. Phys., 13, 2063–2090, https://doi.org/10.5194/acp-13-2063-2013, 2013.

Yukimoto, S., Kawai, H., Koshiro, T., Oshima, N., Yoshida, K., Urakawa, S., Tsujino, H., Deushi, M., Tanaka, T., Hosaka, M., Yabu, S., Yoshimura, H., Shindo, E., Mizuta, R., Obata, A., Adachi, Y., and Ishii, M.: The meteorological research institute Earth system model version 2.0, MRI-ESM2.0: Description and basic evaluation of the physical component, J. Meteorol. Soc. Jpn., 97, 931–965, https://doi.org/10.2151/jmsj.2019-051, 2019.

Zhang, J., Wu, T., Zhang, F., Furtado, K., Xin, X., Shi, X., Li, J., Chu, M., Zhang, L., Liu, Q., Yan, J., Wei, M., and Ma, Q.: BCC-ESM1 Model Datasets for the CMIP6 Aerosol Chemistry Model Intercomparison Project (AerChemMIP), Adv. Atmos. Sci., 38, 317–328, https://doi.org/10.1007/s00376-020-0151-2, 2021.

Zheng, B., Chevallier, F., Yin, Y., Ciais, P., Fortems-Cheiney, A., Deeter, M. N., Parker, R. J., Wang, Y., Worden, H. M., and Zhao, Y.: Global atmospheric carbon monoxide budget 2000–2017 inferred from multi-species atmospheric inversions, Earth Syst. Sci. Data, 11, 1411–1436, https://doi.org/10.5194/essd-11-1411-2019, 2019.